Geoderma 241–242 (2015) 87–96

Contents lists available at ScienceDirect

Geoderma

journal homepage: www.elsevier.com/locate/geoderma

Simulation of soil water and salt transfer under mulched furrow irrigation with saline water

Li-Juan Chen [a,*], Qi Feng [a], Feng-Rui Li [a], Chang-Sheng Li [b]

[a] Cold and Arid Regions Environmental and Engineering Research Institute, Chinese Academy of Sciences, Lanzhou 730000, China
[b] Plant Protection and Quarantine Station of Gansu Province, Lanzhou 730020, China

ARTICLE INFO

Article history:
Received 13 February 2014
Received in revised form 31 October 2014
Accepted 7 November 2014
Available online 22 November 2014

Keywords:
Modeling
Soil water
Soil salt
Furrow irrigation
Saline water irrigation
HYDRUS-2D

ABSTRACT

A mathematical model for simulating soil water and salt transfer under mulched furrow irrigation with saline water was presented. The model performance was evaluated by comparing the simulated values with observed data from the field experiment. The results demonstrated that the model performed reliably in the simulation of water and salt transfer under field conditions. In addition, the model was also used to simulate the process of soil water and salt transfer after saline water irrigation. The simulation demonstrated that the increment of soil water storage below the bottom of the furrow was nearly equal to the value below the top of the ridge immediately after the end of the irrigation (17 h) when the downward movement of irrigation water was restricted by the clay interlayer in soil. However, during the irrigation interval (192 h and 384 h after the irrigation), more water was maintained below the top of the ridge due to a considerable reduction of evaporation under mulched furrow irrigation. Soil salt mainly comes from saline water irrigation and the soil salt below the top of the ridge mainly increased at the redistribution phase (17 h). During the irrigation interval, soil conductivity in surface soil layer below the top of the ridge was smaller than that below the bottom of the furrow, which indicated that the distribution of soil salt below the top of the ridge was more uniform than below the furrow. The model presented here offers an efficient approach to estimate environmental effects of mulched furrow irrigation technology associated to saline water utilization.

© 2014 Elsevier B.V. All rights reserved.

1. Introduction

Saline water, which is in plentiful supply in the world (Mantell et al., 1985), is an important substitutable resource for fresh water in regions with scarce irrigation water of good quality (Pereira et al., 2002). In most arid regions of northwest China, saline water utilization for agriculture is generally combined with surface irrigation. Furrow irrigation with plastic mulching is currently the most common irrigation practice for this combination.

Evaluation of environmental impacts of the combined irrigation practices requires accurate estimation of water and salt fluxes within soil (Crevoisier et al., 2008). In traditional furrow irrigation, salts tend to accumulate in surface soil layers below the ridges (Saggu and Kaushal, 1991) because leaching occurs primarily below the furrows. For mulched furrow irrigation, however, the plastic mulching may induce pronounced changes in soil water flow and salt transfer paths (Zhou et al., 2009; Bezborodov et al., 2010). Based on this consideration, we carried out field experiments to investigate the distributions of soil water and salt under mulched furrow irrigation with saline water. The result showed that salt concentration in surface soil below the ridge was smaller than that below the bottom of the furrow. However, the experiments could not completely explain the cause of the result because of its restriction of observation. Therefore, specialized and efficient methods which could elaborate soil water and salt transfer process are necessary.

Numerical simulation is a proper approach for investigating the process of water and salt movement laterally and vertically away from the bottom of the furrow and allows more flexible representation of the flow domain, boundary conditions, and soil properties than can be achieved in field tests (Warrick, 2003). Numerous models have been developed for simulating water flow and solute transfer under furrow irrigation (e.g., Burguete et al., 2009; Abbasi et al., 2004; Mailhol et al., 2001), but not much is concerning about the effect of plastic covering on the soil, especially under the condition of saline water irrigation. Humberto and Lal (2007) showed that saturated hydraulic conductivity of mulched treatments was 123 times greater and retained 40 to 60% more water than the un-mulched treatment. This modified soil microenvironment which is caused by plastic mulching needs to be recognized when estimating the wetted soil volume and the accumulation of salts in the root zone. Therefore, it is essential to construct a model that accurately represents the actual patterns of soil water flow and salt transfer when using mulched furrow irrigation with saline water.

* Corresponding author.
E-mail addresses: ljchen@lzb.ac.cn, chenlj2001@126.com (L.-J. Chen).

http://dx.doi.org/10.1016/j.geoderma.2014.11.007
0016-7061/© 2014 Elsevier B.V. All rights reserved.

The objective of the study is to establish a mathematical model which is used for simulating soil water and salt transfer under mulched furrow irrigation with saline water. The performance of the model was evaluated by comparing the simulated values with the experimental data. Finally, the process of soil water and salt transfer after irrigation was elaborated in order to explain the differences of soil water and salt distributions below the top of the ridge and the bottom of the furrow. The model could be then used to estimate the environmental effects of mulched furrow irrigation technology associated to saline water utilization.

2. Materials and methods

2.1. Field experiment

We conducted a field experiment at the Test and Demonstration Base for Agricultural Water-saving and Ecological Construction (103°12′03.4″E, 38°42′40.2″N) in Minqin County, Gansu Province, China, from April 22 to September 25, 2013. The experimental site is located at the boundary of Tengger Desert, where average annual evaporation (more than 2664 mm) is twenty four times greater than the annual precipitation (110 mm). The average annual temperature is 7.8 °C, and winter temperature minima can fall to −27.3 °C whereas summer maxima rise to 41.1 °C. The groundwater table is generally below 18 m. The experimental soil is classified as sandy loam in the upper 60 cm with an average bulk density of 1.55 $g\cdot cm^{-3}$, clay in the 60–100 cm layer with an average bulk density of 1.46 $g\cdot cm^{-3}$ and sand in the 100–120 cm layer with an average bulk density of 1.63 $g\cdot cm^{-3}$.

A furrow irrigation system mulched with plastic film (black polyethylene) was used to deliver saline water with an electrical conductivity (EC_w) of 4.46 $dS\cdot m^{-1}$ to Maize (*Yu 22*). Three replications were adopted for the test, and irrigation water was obtained by mixing the water from two wells in specified proportions. One well was located at the experimental station (fresh water (FW), $EC_w = 1.09\ dS\cdot m^{-1}$) and the other was in Huanghui Village (103°36′11.9″E, 39°02′56.4″N) in the Minqin County (saline water (SW), $EC_w = 15.92\ dS\cdot m^{-1}$). The ion concentrations of the source water are presented in Table 1. The desired salinities were obtained as follows:

$$M = \frac{M_f \times Q_f + M_s \times Q_s}{Q_f + Q_s} \quad (1)$$

where M is the salinity of the irrigation water after mixing ($dS\cdot m^{-1}$), M_f is the salinity of the FW ($dS\cdot m^{-1}$), M_s is the salinity of the SW ($dS\cdot m^{-1}$), Q_f is the amount of FW ($m^3\cdot ha^{-1}$), and Q_s is the amount of SW ($m^3\cdot ha^{-1}$).

Three large tanks were used to store the irrigation water: the first and second tanks were filled with water from FW and SW, respectively, and the third was filled with mixing water. The irrigation water was supplied by a pump in amounts that were controlled by valves, with the exact amounts of water supplied monitored by water meters (Fig. 1). The total irrigation volume was 360 mm of irrigation depth (3600 $m^3\cdot ha^{-1}$), which was applied in five irrigation events. According to local irrigation practice, the source water of the first irrigation event was surface water which was supplied from Hongyashan Reservoir by channels ($EC_w = 0.52\ dS\cdot m^{-1}$, see Table 1). The date for this irrigation was on June 2 and the volume of water applied was 45 mm of irrigation depth. The schedule for other four irrigation events with saline water ($EC_w = 4.46\ dS\cdot m^{-1}$) was: June 21, 75 mm; July 9, 75 mm; July 25, 90 mm; and August 12, 75 mm. The average irrigation interval was 17.75 days.

After the experimental field was divided into plots (3 plots, each 12 m long and 3 m wide; Fig. 1), three groups of mulched furrow irrigation system were arranged on each plot. The furrows were closed at the end of the plot to withhold the water. The ridge and furrow for any group were 60 cm wide (30 cm high) and 40 cm wide (30 cm high), respectively. After the plots were mulched with a plastic film (extending for a width of 90 cm), two rows of maize were planted on any ridge with dibblers (the plant density was approximately 45 $kg\cdot ha^{-1}$). The plastic film was joined at the bottom of the furrow and a 10 cm space without plastic film was maintained for water infiltration. This is a common irrigation practice followed by the farmers of the locality. Irrigation was applied in the furrow and the date of application, amount of fertilizer used, use of pesticides, and the undertaking of other necessary operations were prescribed according to typical local practices and general recommendations.

Data relating to precipitation were obtained from the standard meteorological observation station of the base. During each irrigation period, the depth of irrigation water in furrow was recorded once in every 10 min. Soil samples were collected using an auger in the center of each plot before and after each irrigation event. The depth of sampling ranged from 30 cm to 120 cm below the bottom of the furrow (30–40 cm, 40–60 cm, 60–80 cm, 80–100 cm, 100–120 cm) and 0 cm to 120 cm below the top of the ridge (0–20 cm, 20–40 cm, 40–60 cm, 60–80 cm, 80–100 cm, 100–120 cm, Fig. 2). All soil samples were divided into two parts. One part was used for measuring soil water contents by the gravimetric method and another part was used for preparing dilute soil extract solutions. Samples for the solutions were air dried and sieved through a 1 mm mesh. Soluble salt estimates were based on extracts with a 1:5 soil: water ratio, determined using a conductivity meter ($EC_{1:5}$, $dS\cdot m^{-1}$). Soil samples with a wide range of $EC_{1:5}$ values were selected to measure the conductivity of saturated paste extract (EC_e) and the relationship between EC_e and $EC_{1:5}$ was developed subsequently. The conductivities were highly correlated ($R^2 = 0.966$). Thus, EC_e was estimated for all samples using Eq. (2):

$$EC_e = 5.8605 \times EC_{1:5} + 1.3542. \quad (2)$$

The EC_e was converted to salt concentration (C_{sw}, $g\cdot L^{-1}$) using the relationship according to Xin et al. (1986):

$$C_{sw} = 0.67 \times EC_e. \quad (3)$$

Salt concentrations were converted to solute densities ($g\cdot cm^{-3}$) using the measured soil bulk density and volumetric water content.

Soil evaporation was measured using microlysimeters, which were installed at the bottom of the furrow. The microlysimeters were made of two iron tubes with an internal diameter of 15 cm and a depth of 35 cm for the inner and 20 cm and 40 cm for the outer. For each inner tube, the bottom was beveled and a hand auger coupled to the upper part made for easy insertion and removal. After each irrigation event and significant precipitation, the inner tube was inserted into the soil

Table 1
Chemical composition of source water used in the experiment.

Water	HCO_3^- ($mg\cdot L^{-1}$)	Cl^- ($mg\cdot L^{-1}$)	SO_4^{2-} ($mg\cdot L^{-1}$)	Ca^{2+} ($mg\cdot L^{-1}$)	Mg^{2+} ($mg\cdot L^{-1}$)	Na^+ ($mg\cdot L^{-1}$)	K^+ ($mg\cdot L^{-1}$)	TDS ($mg\cdot L^{-1}$)	EC_w ($dS\cdot m^{-1}$)
FW	267	93	307	97	40	109	7.0	921	1.09
SW	689	2906	6334	438	1043	2655	33.6	14,099	15.92
Surface water	150	29	126	41	13	64	2.0	425	0.52

FW is the fresh water from the well located at the experimental station; SW is the saline water from the well located at Huanghui Village; TDS is the total dissolved solids; and EC_w is the electrical conductivity.

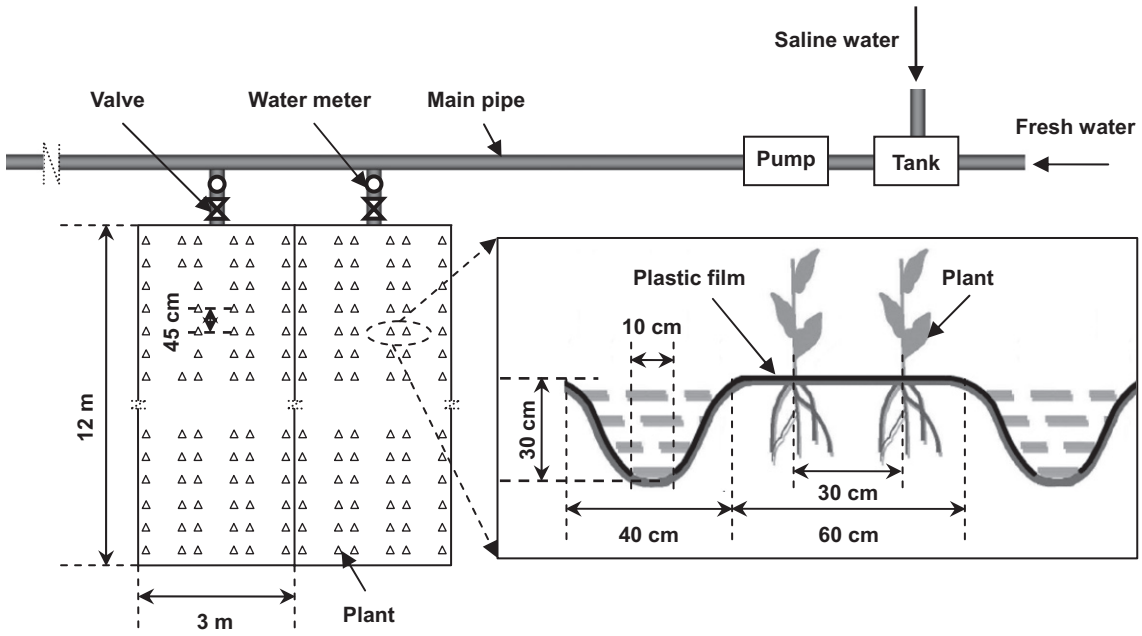

Fig. 1. Layout of the mulched furrow irrigation system with saline water.

and removed with the soil inside intact. Then, the outer tube with open bottom was inserted into the soil. The bottom of each inner tube was sealed with a plastic sheet, weighed, and installed in the outer tube. In order to make the surface of the soil in the inner tube and the surrounding soil surface at the same elevation, the soil in the outer tube should be removed partly. Each inner tube was removed daily from the outer tube and weighed to calculate soil evaporation from mass loss and then returned to their locations. All measurements were performed using an electronic balance with a 0.01 g resolution at 08:00 am.

All data were analyzed using PASW Statistics 18.0 and Surfer 8.0.

2.2. Model development

2.2.1. Mathematical model

We simulated soil water flow and salt transport using HYDRUS-2D (Simunek et al., 1999). Assuming a homogeneous and isotropic soil, the governing equation for water flow can be written as follows:

$$\frac{\partial\theta}{\partial t}=\frac{\partial}{\partial x}\left[K(h)\frac{\partial h}{\partial x}\right]+\frac{\partial}{\partial z}\left[K(h)\frac{\partial h}{\partial z}\right]+\frac{\partial K(h)}{\partial z}-S \tag{4}$$

where θ is the volumetric water content of the soil ($cm^3 \cdot cm^{-3}$), t is the time (d), x is the radial coordinate (cm), $K(h)$ is the hydraulic conductivity ($cm \cdot d^{-1}$), h is the pressure head (cm), z is the vertical coordinate taken positive upwards (cm), and S is a distributed sink function representing water uptake by the roots ($1 \cdot d^{-1}$).

In our model, solute transport was described as follows:

$$\frac{\partial(\theta c)}{\partial t}=\frac{\partial}{\partial x}\left(\theta D_{xx}\frac{\partial c}{\partial x}\right)+\frac{\partial}{\partial x}\left(\theta D_{xz}\frac{\partial c}{\partial z}\right)+\frac{\partial}{\partial z}\left(\theta D_{zz}\frac{\partial c}{\partial z}\right)+\frac{\partial}{\partial z}\left(\theta D_{zx}\frac{\partial c}{\partial x}\right)-\frac{\partial}{\partial x}(q_x c)-\frac{\partial}{\partial z}(q_z c) \tag{5}$$

where c is the concentration of the solute in the soil solution ($g \cdot cm^{-3}$), D is the dispersion coefficient ($cm^2 \cdot d^{-1}$), and q is the volumetric flux density ($cm \cdot d^{-1}$).

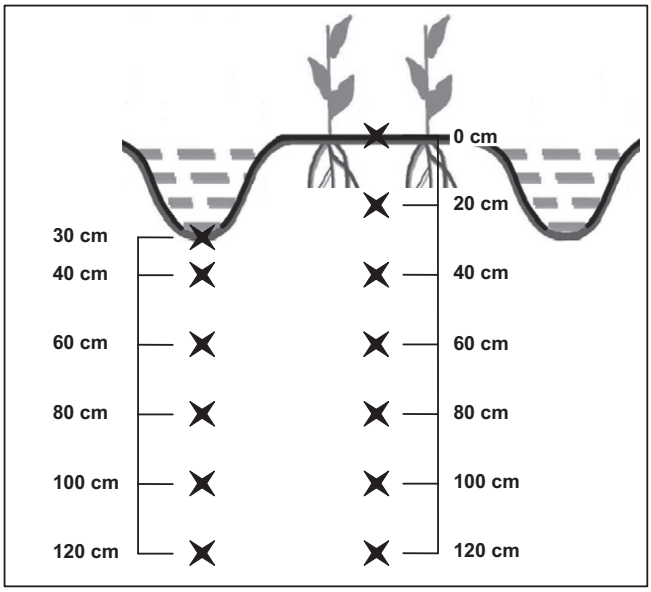

Fig. 2. Locations of the sampling sites.

2.2.2. Initial and boundary conditions

The origin of the coordinates ($x = 0$ and $z = 0$) was placed at the center of the furrow, as illustrated by the schematic diagram presented in Fig. 3.

Measured soil water pressure heads $h_0(r, z)$ and soil salinities $c_0(h, z)$ (collected on June 20, before the first saline water irrigation event) were used as initial conditions within the flow domain. Then,

$$h(x,z,t)=h_0(x,z),\ \ c(x,z,t)=c_0(x,z),\ \ t=0,\ \ 0\le x\le X,\ \ 0\le z\le Z \tag{6}$$

where X and Z are the maximum horizontal and vertical lengths of simulated domain (cm).

We divided each irrigation event into two phases: the irrigation phase (the time from irrigation event began to water pond disappeared in the furrow) and soil water redistribution phase (the time from water pond disappeared in the furrow to next irrigation event began). During each irrigation phase, there was a time variable boundary condition at the bottom of the furrow when pressure head changed with irrigation

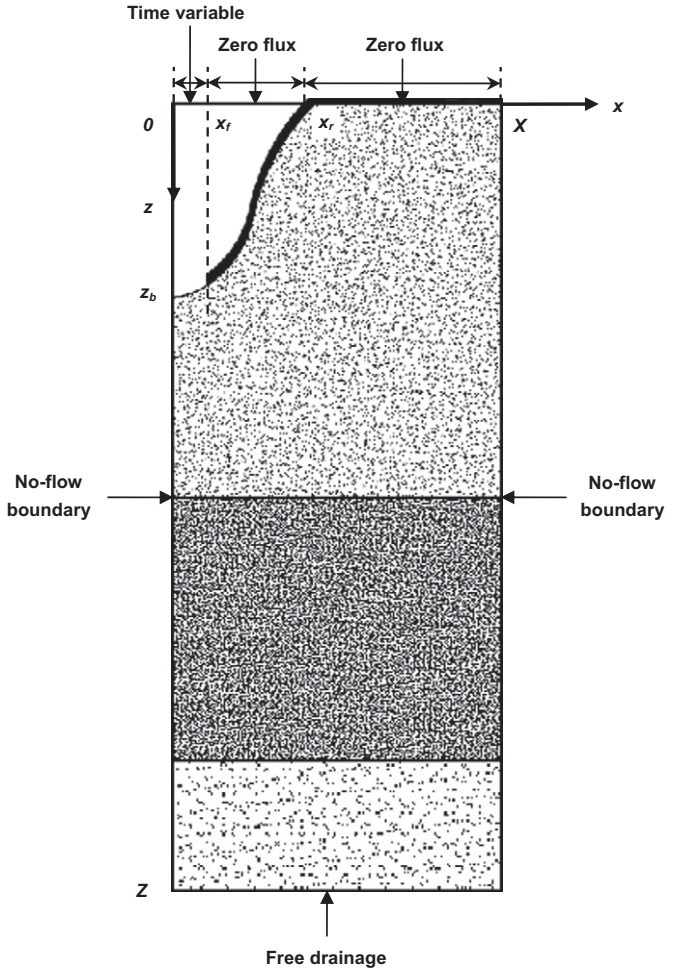

Fig. 3. The schematic diagram of the model. The soil is classified as sandy loam in the upper 60 cm, clay in the 60–100 cm layer and sand in the 100–120 cm layer.

time ($h(x,t)$). The solute flux was deduced from the irrigation water salinity and the amount of irrigation, as follows:

$$-K(h)\frac{\partial h}{\partial z}+K(h)=h(x,t),\quad -\theta D\frac{\partial c}{\partial z}+qc = \varepsilon c_R,\quad 0<t<t_a,\quad 0\le x\le x_f,\quad z=z_b \tag{7}$$

where t_a is the time during each irrigation event (d), x_f is the left side of plastic film (cm), ε is the volumetric flux density of irrigation ($cm\cdot d^{-1}$), c_R is the salinity of irrigation water ($g\cdot cm^{-3}$), and z_b is the depth of the furrow.

During each soil water redistribution phase, an atmospheric boundary condition was imposed at the bottom of the furrow:

$$-K(h)\frac{\partial h}{\partial z}+K(h)=E_f,\quad -\theta D\frac{\partial c}{\partial z}+qc=0,\quad t>t_a,\quad 0\le x\le x_f,\quad z=z_b \tag{8}$$

where E_f is the evaporation of soil ($cm\cdot d^{-1}$), which was measured by the microlysimeters.

Beyond the bottom of the furrow, because of the plastic mulching, there was a zero flux boundary condition:

$$-K(h)\frac{\partial h}{\partial x}-K(h)\frac{\partial h}{\partial z}+K(h)=0,\quad -\theta D\frac{\partial c}{\partial z}+qc = 0,\quad t>0,\quad x_f<x\le x_r,\quad 0\le z<z_b \tag{9}$$

where x_r is the boundary of the furrow and the ridge (cm).

A zero flux boundary condition was also imposed on the ridge owing to the plastic mulching (soil evaporation was less than 5% of the water application rate during irrigation and was reduced to low levels after irrigation):

$$-K(h)\frac{\partial h}{\partial z}+K(h)=0,\quad -\theta D\frac{\partial c}{\partial z}+qc=0,\quad t>0,\quad x_r<x\le X,\quad z=0. \tag{10}$$

Finally, because the groundwater table of the experimental field lies below the domain of interest (i.e., approximately 18.0 m below the soil surface), the free drainage bottom boundary condition was used for both water flow and solute transport.

For the simulation, it was assumed that no flow of water or salt took place along the two perpendicular sides of the flow domain. Accordingly, we enforced a no-flow boundary condition for these regions.

2.3. Parameters and simulation inputs

In our simulations, $X = 50$ cm, $Z = 120$ cm, $x_f = 5$ cm, $x_r = 20$ cm, and $z_b = 30$ cm. The soil profiles were classified as sandy loam, clay and sand according to experimental soil (Fig. 3). Undisturbed soil samples were collected at the beginning of the experiment from different soil layers within the soil profiles to measure soil hydraulic properties. The soil water characteristic curve and hydraulic conductivity were determined in the laboratory using a soil moisture suction measuring meter (SXY-2, China) and an unsaturated hydraulic conductivity measuring meter (FS-1, China), respectively. The average values obtained for the measured parameters are presented in Table 2.

According to Ramos et al. (2011), potential root water uptake can decrease in response to water stress. Here, we described the reduction due to water stress using the model developed by Feddes et al. (1978):

$$\alpha(h)=\begin{cases}0 & h\ge h_1 \quad or \quad h\le h_4\\ \dfrac{h-h_1}{h_2-h_1} & h_2<h<h_1\\ 1 & h_3\le h\le h_2\\ \dfrac{h-h_4}{h_3-h_4} & h_4<h<h_3\end{cases} \tag{11}$$

where h_1, h_2, h_3, and h_4 are the threshold parameters, which were taken from the HYDRUS-2D internal database (i.e. $h_1 = -15$ cm, $h_2 = -30$ cm, $h_3 = -325$ cm, and $h_4 = -8000$ cm).

Solute transport parameters were obtained from solute displacement experiments conducted on undisturbed cylindrical samples. Further details can be found in a previous study by Ramos et al. (2011).

The precipitation was obtained from the standard meteorological observation station of the base (Fig. 4), and the soil evaporation used

Table 2
Water transfer parameters of the Van Genuchten water retention curves.

Depth (cm)	Soil	K_s ($cm\cdot d^{-1}$)	θ_s ($cm^3\cdot cm^{-3}$)	θ_r ($cm^3\cdot cm^{-3}$)	a ($1\cdot cm^{-1}$)	n	l
0–60	Sandy loam	45.85	0.382	0.072	0.0121	1.408	0.5
60–100	Clay	10.19	0.398	0.096	0.0156	1.565	0.5
100–120	Sand	104.08	0.346	0.035	0.0283	1.488	0.5

K_s is the saturated hydraulic conductivity; θ_s is the saturated water content; θ_r is the residual water content; a and n are retention curve shape parameters; and l is the pore connectivity parameter.

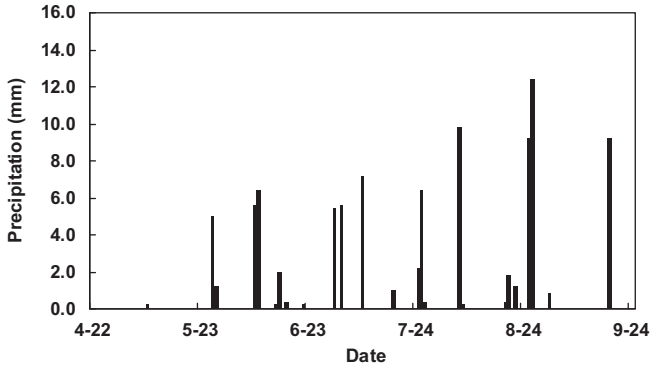

Fig. 4. Precipitation during the growth period of maize in 2013.

for the atmospheric boundary condition was determined using the microlysimeters. Initial soil water and salt contents were based on measurements obtained in the field (Table 3). The presented application assumes a longitudinal dispersivity of 5.0 cm, with a transverse dispersivity being one-tenth of the longitudinal dispersivity, and neglects molecular diffusion. Our simulations were carried out for all saline water irrigation and redistribution periods (from June 20 to August 30). The schedule of irrigation was consistent with the field experiment. For each irrigation event, the liquid water remained pooled in the furrows for 5.1, 8.2, 8.5, 9.9 and 8.7 h, respectively.

In order to model soil solute transfer it was assumed that the solutes were non-reactive and there was no net precipitation or dissolution (e.g., Skaggs et al., 2006; Ramos et al., 2011; Wang et al., 2014). These studies demonstrated that this approach can be successfully used under irrigation environments. Additionally, Ramos et al. (2011) reported that similar salinity distributions were obtained when this approach using HYDRUS was compared with much more complex predictions involving consideration of precipitation/dissolution and ion exchange as done with UNSATCHEM.

2.4. Statistical analysis

To evaluate the model performance for simulation, three different statistical indexes were used. The first two indexes, the mean absolute error (MAE) and the root mean square error (RMSE) reflect the differences between observations and simulations. They were calculated as follows:

$$\mathrm{MAE} = \frac{1}{n}\sum_{i=1}^{n}|Y_{io} - Y_{ie}| \tag{12}$$

$$\mathrm{RMSE} = \sqrt{\frac{1}{n}\sum_{i=1}^{n}(Y_{io} - Y_{ie})^2} \tag{13}$$

where Y_{io} and Y_{ie} are the observed and simulated values and n is the number of pair values.

To describe the processes of soil water flow and salt transport, the soil water/salinity concentration storage increment (ΔS_i) and the rate of soil water/salinity concentration storage increment (R_i) were used, which were calculated as:

$$\Delta S_i = \psi_i - \psi_{i0} \tag{14}$$

$$R_i = \frac{\Delta S_i}{\sum_{i=1}^{z_m}(\psi_i - \psi_{i0})} \tag{15}$$

where Ψ_i is the soil water/salinity concentration storage at the depth of i (e.g. 0–20 cm below the top of the ridge) at a certain time (e.g. 1.35 h) after irrigation, Ψ_{i0} is the initial soil water/salinity concentration storage at the depth of i before irrigation, z_m is the depth from the soil surface to the reference depth (30–120 cm below the bottom of the furrow and 0–120 cm below the top of the ridge).

3. Results and discussion

3.1. Simulated versus observed results

The simulated values of soil water content and salinity concentration during the simulation period were compared graphically with the observed results for different depths corresponding to those of the experimental observations (Fig. 5). While there were some differences between the simulations and observations, overall, the simulations were very good. For all of the saline water irrigation applications, both the observations and simulations showed simultaneous increases in soil water content at a depth of 0–60 cm below the top of the ridge and 30–60 cm below the bottom of the furrow after irrigation. In addition, they presented instantaneous responses during soil water redistribution phases. The performance of the model in simulating soil water content at 60–100 cm was slightly poor (Fig. 5a and b). The dynamics for the simulations coincided with the upper soil layers, while for the observations were random. This deviation revealed the complexion of soil water movement in the interface of sandy loam and clay in the field. The restrictive assumptions which were made during the establishment of the model made the perfect coincidences unlikely. For statistical comparison, however, the difference between the simulated and measured soil water contents, i.e., the mean absolute error (MAE) and the root-mean-square-error (RMSE), ranged from 0.0099 to 0.0328 $cm^3 \cdot cm^{-3}$ and 0.0129 to 0.0370 $cm^3 \cdot cm^{-3}$, respectively (Table 4).

The simulated soil salinity concentration showed regular changes at 0–60 cm below the top of the ridge and 30–60 cm below the bottom of the furrow after the first saline water irrigation, which was different from observations (72 h in Fig. 5c and d). One possible explanation is the fact that the plant can absorb a small amount of soil salt during the simulation period, which was neglected in simulation. After the

Table 3
Initial and average soil water and salt contents below the top of the ridge and the bottom of the furrow.

Below the top of the ridge					Below the bottom of the furrow				
Depth (cm)	IW ($cm^3 \cdot cm^{-3}$)	AW ($cm^3 \cdot cm^{-3}$)	IS ($g \cdot L^{-1}$)	AS ($g \cdot L^{-1}$)	Depth (cm)	IW ($cm^3 \cdot cm^{-3}$)	AW ($cm^3 \cdot cm^{-3}$)	IS ($g \cdot L^{-1}$)	AS ($g \cdot L^{-1}$)
0–20	0.193	0.241	1.638	3.676	–	–	–	–	–
20–40	0.257	0.254	1.665	3.770	30–40	0.225	0.294	1.712	4.512
40–60	0.210	0.213	1.465	2.926	40–60	0.242	0.280	1.873	3.236
60–80	0.134	0.117	1.375	2.022	60–80	0.123	0.131	1.677	2.140
80–100	0.157	0.113	1.257	1.708	80–100	0.114	0.111	1.272	1.740
100–120	0.286	0.283	1.626	2.070	100–120	0.273	0.283	1.579	2.066

IW is the initial soil water content; AW is the average soil water content during the growth period; IS is the initial soil salinity concentration; and AS is the average soil salinity concentration during the growth period.

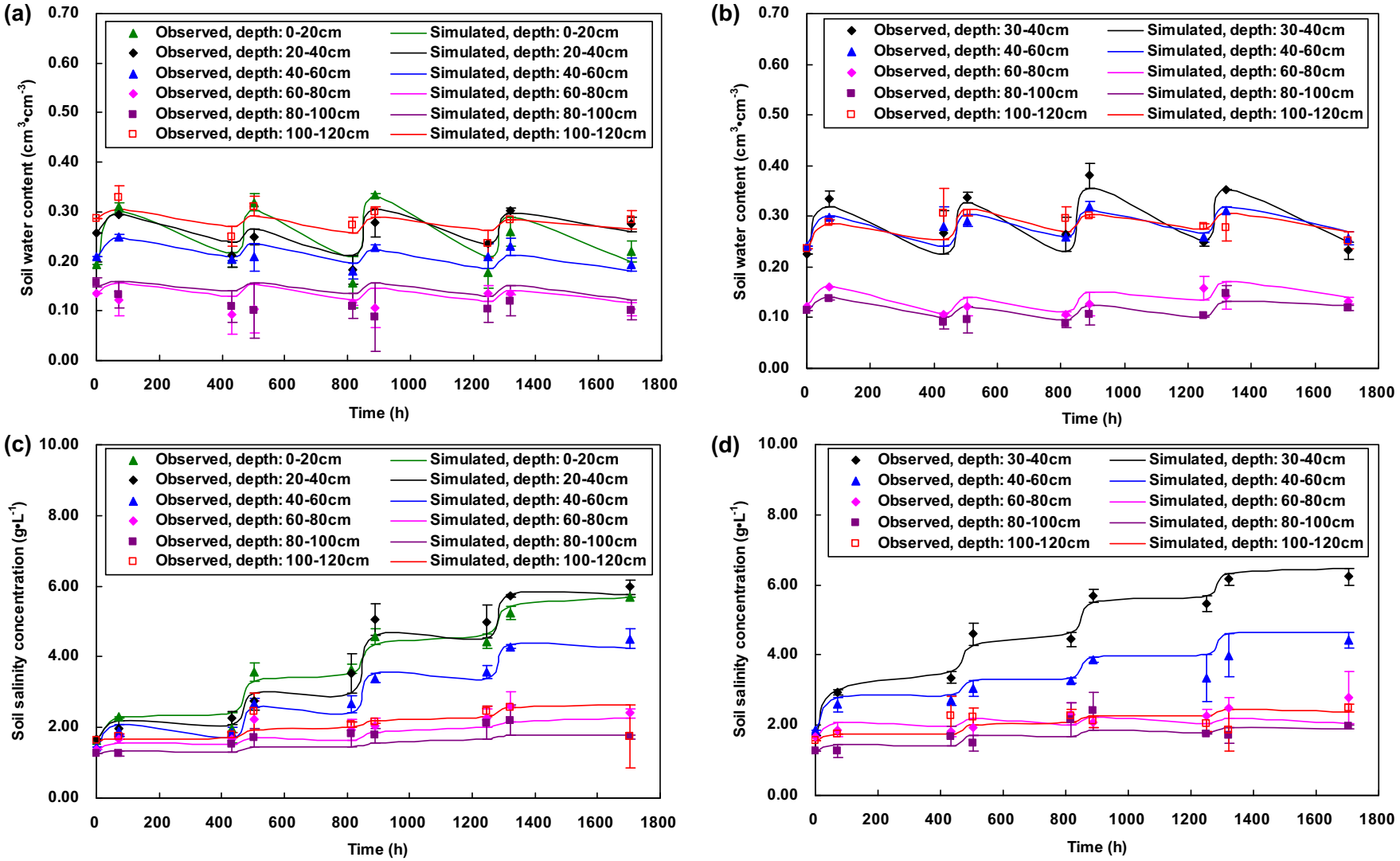

Fig. 5. Simulated and observed soil water content below the top of the ridge (a) and the bottom of the furrow (b), and soil salinity concentration below the top of the ridge (c) and the bottom of the furrow (d). The simulation duration was 75 days (from June 20 at 8:00 am to August 30 at 8:00 am).

Table 4
Results of the statistical analysis between measured and simulated soil water and salt contents.

Statistics	Below the top of the ridge			Below the bottom of the furrow		
	Depth (cm)	Soil water content ($cm^3 \cdot cm^{-3}$)	Soil salinity concentration ($g \cdot L^{-1}$)	Depth (cm)	Soil water content ($cm^3 \cdot cm^{-3}$)	Soil salinity concentration ($g \cdot L^{-1}$)
MAE	0–20	0.0198	0.1588	–	–	–
	20–40	0.0133	0.2635	30–40	0.0168	0.1763
	40–60	0.0123	0.1488	40–60	0.0099	0.2456
	60–80	0.0220	0.2354	60–80	0.0121	0.2565
	80–100	0.0328	0.2280	80–100	0.0100	0.2234
	100–120	0.0154	0.2011	100–120	0.0153	0.2277
RMSE	0–20	0.0250	0.2067	–	–	–
	20–40	0.0176	0.3198	30–40	0.0217	0.1968
	40–60	0.0154	0.1719	40–60	0.0150	0.3314
	60–80	0.0279	0.2834	60–80	0.0159	0.3204
	80–100	0.0370	0.2774	80–100	0.0129	0.2889
	100–120	0.0180	0.3493	100–120	0.0217	0.3034

MAE, the mean absolute error; RMSE, the root mean square error.

third irrigation (888 h in Fig. 5 d), the differences between the observations and simulations were much higher at 30–40 cm and 40–60 cm below the bottom of the furrow. For example, the soil salinity concentration at 40 — 60 cm for observations were 3.34 $g \cdot L^{-1}$ at 1248 h, 3.99 $g \cdot L^{-1}$ at 1320 h and 4.41 $g \cdot L^{-1}$ at 1704, while for simulations were 4.01, 4.60 and 4.63 $g \cdot L^{-1}$, respectively. This is because the bigger amount of the third irrigation (90 mm of irrigation depth) leached the soil salt slightly, which made the observations lower than the simulations. For statistical comparison, the MAE and RMSE ranged from 0.1488 to 0.2635 $g \cdot L^{-1}$ and 0.1719 to 0.3493 $g \cdot L^{-1}$ (Table 4) for the entire simulating period, for all depths and both below the top of the ridge and the bottom of the furrow. Based on these values, we conclude that our model reproduces water flow and salt transport under field conditions reliably.

3.2. Soil water flow during irrigation and redistribution phase

The processes of soil water movement after the first saline water irrigation (June 21) are illustrated in Fig. 6. During the irrigation phase, soil water moved in both vertical and horizontal directions. The total amount of irrigation water (75 mm of irrigation depth) was delivered in a short time (1.35 h) but cannot infiltrate fast enough into the surrounding soil. Therefore, water accumulated in the furrow. At 8.2 h, there was no water left in the furrow. During the redistribution phase, the maximum soil water content below the top of the ridge appeared at 17 h. Fig. 6 presents the variation in soil water distribution patterns at six different times: one day before the irrigation (panel a), irrigation duration (1.35 h, panel b), 8.2 h (panel c), 17 h (panel d), 192 h (panel e) and 384 h (panel f).

From Fig. 6a–c it can be seen that soil water movements in the upper 60 cm below the top of the ridge and 30–60 cm below the bottom of the furrow were strong than lower layers. At 1.35 h, the rate of soil water storage increment was 53.37% at 30–60 cm below the bottom of the furrow and 30.18% at 0–60 cm below the top of the ridge, respectively. At 8.2 h, above values were 36.47% and 38.68%, respectively. This could be attributed to the limitation of the soil infiltration rate in clay soil (60–100 cm). The processes of swelling, dispersion, and movement of clay particles resulted in pore blockage in soil (Frenkel et al., 1978) which restricted downward water infiltration. As a result, horizontal soil water movement was enhanced and the soil water content below the top of the ridge was increased. From Fig. 6d it can be seen that soil water continually moved from the furrow to the ridge and moved upwards below the top of the ridge during the redistribution phase. The contours of soil water content become straight than before, which indicated that a temporary equilibrium appeared. The rate of soil water storage increment was 51.13% below the bottom of the furrow and 48.87% below the top of the ridge. This result revealed that the increment of soil water storage below the bottom of the furrow was nearly equal to the value below the top of the ridge at this moment.

Fig. 6e and f showed that soil water decreased because of soil evaporation at the bottom of the furrow and the crop transpiration on the ridge. At 192 h, the rates of soil water storage increment below the bottom of the furrow and the ridge were 47.98% and 52.02%, respectively. At 384 h, the decrement of soil water storage below the bottom of the furrow was 7.62 mm, while the increment of soil water storage below the top of the ridge was 1.53 mm. This result revealed that more water was maintained below the top of the ridge during irrigation interval under mulched furrow irrigation.

3.3. Soil salt transfer during irrigation and redistribution phase

Fig. 7 presents the variation in soil salinity concentration at six different times. From Fig. 7a–c it can be seen that soil salinity mainly comes from saline water irrigation. At 1.35 h, the rate of soil salinity concentration storage increment was 73.13% below the bottom of the furrow and 26.88% below the top of the ridge, respectively. At 8.2 h, the soil salinity concentration below the bottom of the furrow was high (3.66 $g \cdot L^{-1}$) in the top 10 cm and dropped to approximately 1.46 $g \cdot L^{-1}$ at a depth of 95 cm and then increased to 1.65 $g \cdot L^{-1}$ at 120 cm. The increment of soil salinity concentration below the bottom of the furrow was 2.72 and 1.75 times greater than that below the top of the ridge at 1.35 h and 8.2 h, respectively. This result indicated that the introduced soil salt primarily accumulated in the furrow surface during the irrigation. Compared with Fig. 6a–c, the movement and redistribution of soil salt were slightly different with soil water. One possible explanation is that the movement of soil salt was lagged behind the movement of soil water. The difference in infiltration rate under each layer could also influence the movement of the soil salt.

At 17 h (Fig. 7d), soil salt moved downwards to the subsoil below the bottom of the furrow as well as to the surface layers below the top of the ridge. The rate of soil salinity concentration storage increment was 55.09% below the bottom of the furrow and 44.91% below the top of the ridge, respectively. It meant that soil salt below the top of the ridge mainly increased at this moment. However, the total increment of soil salinity concentration storage below the top of the ridge was low than that below the bottom of the furrow. During the irrigation interval, soil salt moved upwards below the bottom of the furrow (Fig. 7e and f). At 192 h, the rate of soil salinity concentration storage increment was 30.35% at 30–40 cm (with the total rate of 56.57% at 30–120 cm) below the bottom of the furrow. Because the evaporation reduced considerably under mulched furrow irrigation, the effect of evaporation on

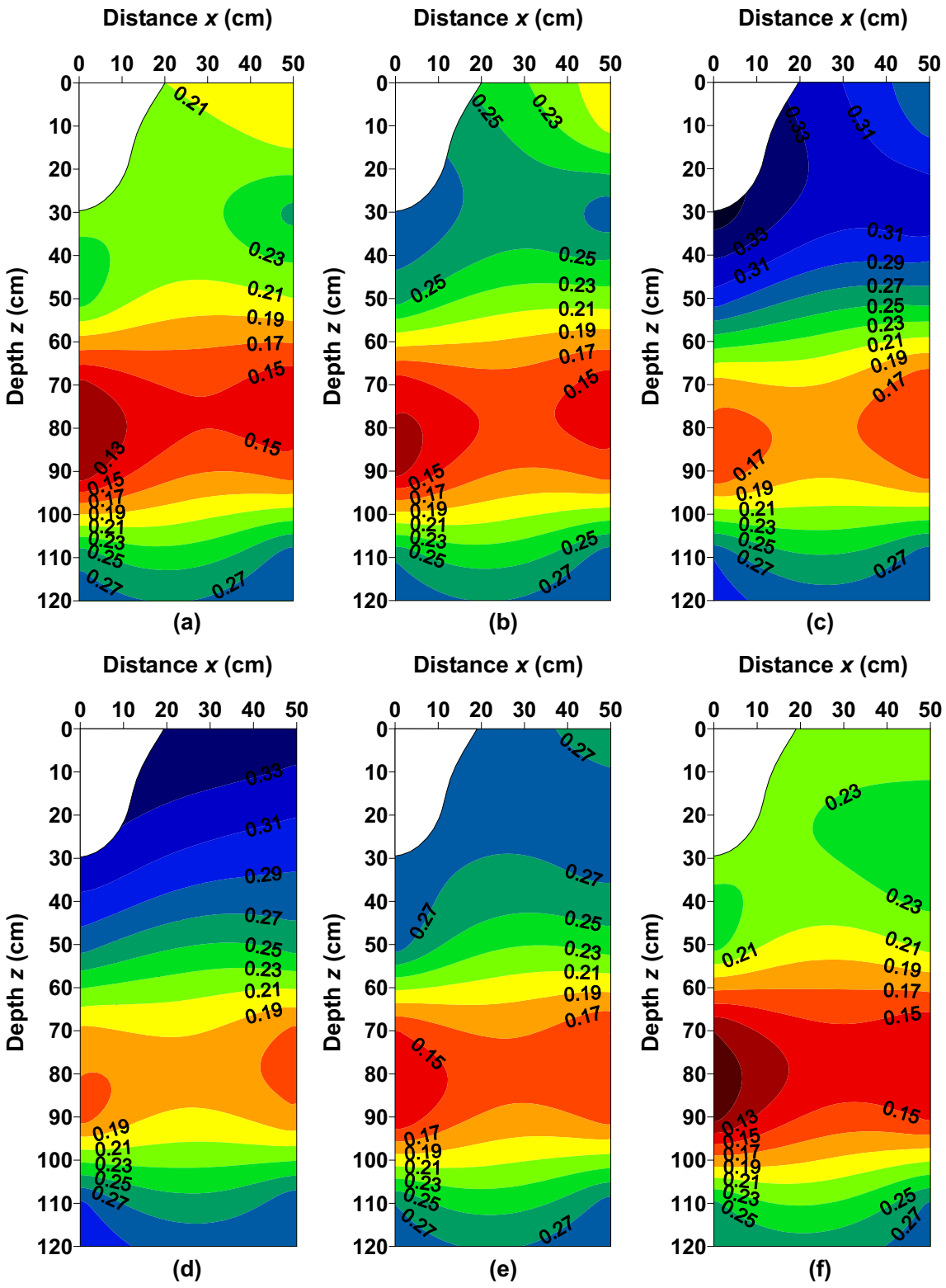

Fig. 6. Spatial distribution of simulated soil water content ($cm^3 \cdot cm^{-3}$) at six different times: one day before (a) and 1.35 h (b), 8.2 h (c), 17 h (d), 192 h (e), and 384 h (f) after the first saline water irrigation (started at 8:00 am on June 21st). The irrigation duration was 1.35 h.

the ridge can be ignored in the process of the salt redistribution. Under the effect of crop transpiration, the rate of soil salinity concentration storage increment was 13.53% at 0–20 cm (with the total rate of 43.43% at 0–120 cm) below the top of the ridge. At 384 h, the rate of soil salinity concentration storage increment was 36.40% at 30–40 cm (with the total rate of 57.60% at 30–120 cm) below the bottom of the furrow and 15.72% at 0–20 cm (with the total rate of 42.40% at 0–120 cm) below the top of the ridge. This result indicated that the distribution of soil salt below the top of the ridge was more uniform than below the furrow. As a result, soil salinity concentration in the surface soil layer below the top of the ridge was smaller than that below the bottom of the furrow.

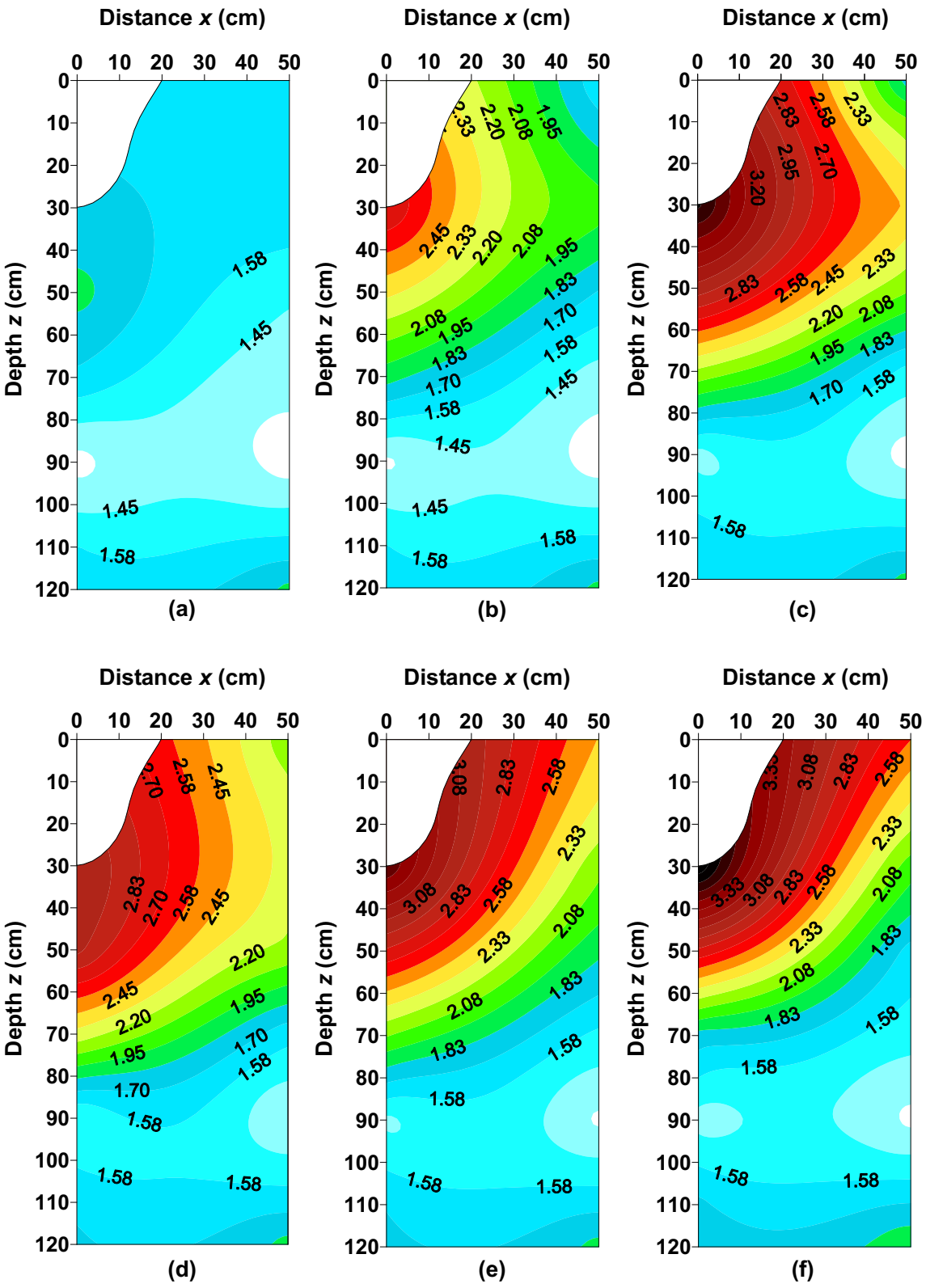

Fig. 7. Spatial distribution of simulated soil salinity concentration ($g \cdot L^{-1}$) at six different times: one day before (a) and 1.35 h (b), 8.2 h (c), 17 h (d), 192 h (e), and 384 h (f) after the first saline water irrigation (started at 8:00 am on June 21st).

4. Conclusions

In the present study, we developed a mathematical model describing soil water and salt transfer under mulched furrow irrigation with saline water. We conducted field experiment in Minqin County, China and used the resulting data to evaluate the performance of our model by comparing the simulated values with the experimental data. The graphical comparison of simulated and observed soil water content demonstrated a similar trend at a soil layer of 0–60 cm throughout the simulation period. The small differences observed at 60–100 cm may

be partially due to different infiltration rates in sandy loam (0–60 cm) and clay (60–100 cm). The statistical (RMSE) comparison revealed an acceptable agreement between measured and simulated soil water contents and salinity concentration. Overall, the differences of soil salinity concentration could be partly explained by the fact that the plant can absorb a small amount of soil salt during the growth period, which was neglected in simulation.

It can be concluded that the model is reliable to reproduce soil water and salt transfer under field conditions. We used the model to simulate the process of soil water and salt transfer after the first saline water irrigation. The results demonstrated that the downward movement of irrigation water was restricted under the effect of clay interlayer in soil, which resulted in soil water and salt transferred mainly in the upper layers (0–60 cm). Therefore, immediately after the end of the irrigation (17 h), the increment of soil water storage below the bottom of the furrow was nearly equal to the value below the top of the ridge. During the irrigation interval, however, more water was maintained below the top of the ridge, which may be due to a considerable reduction of evaporation under mulched furrow irrigation. Our soil salt transfer simulations displayed that soil salinity mainly comes from saline water irrigation. The increment of soil salinity concentration below the bottom of the furrow was 2.72, 1.75 and 1.23 times greater than that below the top of the ridge at 1.35 h, 8.2 h and 17 h, which meant that soil salt below the top of the ridge mainly increased at the redistribution phase. During the irrigation interval, soil salinity concentration in surface soil layer below the top of the ridge was smaller than that below the bottom of the furrow, which indicated that the distribution of soil salt below the top of the ridge was more uniform than below the furrow.

The model presented in this study offers an efficient approach to exploring the mechanisms underlying soil water and salt transfer under mulched furrow irrigation with saline water. It has the potential to be applied to a variety of soil types, water qualities, and water application strategies (e.g., blending, cyclic) and thus is broadly applicable to designing mulched furrow irrigation systems with saline or fresh water.

Acknowledgments

This research was supported by the China Postdoctoral Science Foundation (2013M542407), the Foundation for Excellent Youth Scholars of CAREERI, CAS (Y451051001) and the Key Project of the Chinese Academy of Sciences (Y42AC71001).

References

Abbasi, F., Feyen, J., van Genuchten, M.Th, 2004. Two-dimensional simulation of water flow and solute transport below furrows: model calibration and validation. J. Hydrol. 290, 63–79.

Bezborodov, G.A., Shadmanov, D.K., Mirhashimov, R.T., Yuldashev, T., Qureshi, A.S., Noble, A.D., Qadir, M., 2010. Mulching and water quality effects on soil salinity and sodicity dynamics and cotton productivity in Central Asia. Agric. Ecosyst. Environ. 138, 95–102.

Burguete, J., Zapata, N., García-Navarro, P., Maïkaka, M., Playán, E., Murillo, J., 2009. Fertigation in furrows and level furrow systems. I: model description and numerical tests. J. Irrig. Drain. Eng. 135, 401–412.

Crevoisier, D., Popova, Z., Mailhol, J.C., Ruelle, P., 2008. Assessment and simulation of water and nitrogen transfer under furrow irrigation. Agric. Water Manag. 95, 354–366.

Feddes, R.A., Kowalik, P.J., Zaradny, H., 1978. Simulation of field water use and crop yield. Simulation MonographsPudoc, Wageningen.

Frenkel, H., Goertzen, J.O., Rhoades, J.D., 1978. Effect of clay type and content, exchangeable sodium percentage and electrolyte concentration on clay dispersion and soil hydraulic conductivity. Soil Sci. Soc. Am. J. 42, 32–39.

Humberto, B.C., Lal, R., 2007. Impacts of long-term wheat straw management on soil hydraulic properties under no-tillage. Soil Sci. Soc. Am. J. 71, 1166–1173.

Mailhol, J.C., Ruelle, P., Nemeth, I., 2001. Impact of fertilization practices on nitrogen leaching under irrigation. Irrig. Sci. 20, 139–147.

Mantell, A., Frenkel, H., Meiri, A., 1985. Drip irrigation of cotton with sline-socic water. Irrig. Sci. 6, 95–106.

Pereira, L.S., Cordey, I., Iacovides, I., 2002. Coping With Water Scarcity. Unesco, Paris.

Ramos, T.B., Simunek, J., Goncalves, M.C., Martins, J.C., Prazeres, A., Castanheira, N.L., Pereira, L.S., 2011. Field evaluation of a multicomponent solute transport model in soils irrigated with saline waters. J. Hydrol. 407, 129–144.

Saggu, S.S., Kaushal, M.P., 1991. Fresh and saline water irrigation through drip and furrow method. Int. J. Trop. Agric. 9, 194–202.

Simunek, J., Sejna, M., van Genuchten, M.Th, 1999. The HYDRUS-2D software package for simulating two-dimensional movement of water, heat, and multiple solutes in variable saturated media. Version 2.0. IGWMCTPS-53. International Ground Water Modeling Center, Colorado School of Mines, Golden, Colorado.

Skaggs, T.H., van Genuchten, M.Th., Shouse, P.J., Poss, J.A., 2006. Macroscopic approaches to root water uptake as a function of water and salinity stress. Agric. Water Manag. 86, 140–149.

Wang, Z., Jin, M., Simunek, J., van Genuchten, M.Th., 2014. Evaluation of mulched drip irrigation for cotton in arid Northwest China. Irrig. Sci. 32, 15–27.

Warrick, A.W., 2003. Soil Water Dynamics. Oxford University Press, New York.

Xin, J.F., Zhang, G.Y., Li, Y.Z., 1986. Comparative and relationship of the different methods to expressing soil salinity. Beijing Agricultural University Press, Beijing (in Chinese).

Zhou, L.M., Li, F.M., Jin, S.L., Song, Y., 2009. How two ridges and the furrow mulched with plastic film affect soil water, soil temperature and yield of maize on the semiarid Loess Plateau of China. Field Crop Res. 113, 41–47.